Appl. Sci. **2015**, *5*, 344-358; doi:10.3390/app5030344

OPEN ACCESS

applied sciences

ISSN 2076-3417

www.mdpi.com/journal/applsci

Article

Synthesis, Characterization and Shape-Dependent Catalytic CO Oxidation Performance of Ruthenium Oxide Nanomaterials: Influence of Polymer Surfactant

Antony Ananth [1], Duncan H. Gregory [2] and Young Sun Mok [1,*]

[1] Department of Chemical and Biological Engineering, Jeju National University, Jeju 690-756, Korea; E-Mail: sebastiananananth@gmail.com

[2] School of Chemistry, University of Glasgow, Glasgow G12 8QQ, UK; E-Mail: Duncan.Gregory@glasgow.ac.uk

* Author to whom correspondence should be addressed; E-Mail: smokie@jejunu.ac.kr; Tel.: +82-64-754-3682; Fax: +82-64-755-3670.

Academic Editor: Rajender S. Varma

Received: 26 June 2015 / Accepted: 5 August 2015 / Published: 11 August 2015

Abstract: Ruthenium oxide nano-catalysts supported on mesoporous γ-Al_2O_3 have been prepared by co-precipitation method and tested for CO oxidation. The effect of polyethylene glycol (PEG) on the properties of the catalyst was studied. Addition of the PEG surfactant acted as a stabilizer and induced a change in the morphology of ruthenium oxide from spherical nanoparticles to one-dimensional nanorods. Total CO conversion was measured as a function of morphology at 175 °C and 200 °C with 1.0 wt.% loading for PEG-stabilized and un-stabilized catalysts, respectively. Conversion routinely increased with temperature but in each case, the PEG-stabilized catalyst exhibited a notably higher catalytic activity as compared to the un-stabilized equivalent. It can be assumed that the increase in the activity is due to the changes in porosity, shape and dispersion of the catalyst engendered by the use of PEG.

Keywords: ruthenium oxide; polyethylene glycol; shape effect; CO oxidation

1. Introduction

Ruthenium oxide (RuO_x) is a promising-material both in the context of catalysis [1,2] and energy [3]. For instance, combinations and composites based on metallic ruthenium/ruthenium oxides are notable for coupling reaction catalysis [4], catalyzing the photochemical reduction of water [5], as thin film resistors for inkjet printing [6] and as catalysts for N_2O decomposition [7], selective oxidation of alcohol [8] and oxidation of carbon monoxide (CO) [9–11]. Among the above chemical processes, CO oxidation is an attractive one for study since it is both an industrially important reaction and relatively uncomplicated to model experimentally and computationally. The impact of CO on environmental air quality is considerable and as a toxic gas an exposure of 800 ppm for 1 h is fatal to human life [12]. Noble metal catalysts such as Pt and Pd exhibit good CO oxidation activity but concerns over cost and abundance have compelled researchers to develop metal oxides as a viable alternative [13–16]. The catalytic activity of candidate metal oxide systems is heavily dependent on oxidation state and for example in the Ru-O system, when a RuO_2 catalyst is used under a high partial pressure of O_2, it exhibits a superior CO oxidation performance than metallic Ru catalysts [10,17]. Moreover, the performance of such catalysts can be greatly improved when stabilized or uniformly dispersed on the surface of a suitable support [18–20].

Dispersion is a critical step in furthering an effective reaction between the reactants [21]. Conventional methods of catalyst dispersion on support materials by wet impregnation often yield aggregated structures [22]. Polymers can be used in nanomaterial syntheses as stabilizers, surfactants or growth-directing agents [23,24] in which they control the particle aggregation, pore characteristics and in a catalysis context, the stability and poisoning resistance of the support [25]. Polyethylene glycol (PEG) is one of the most widely-used polymers in the design of heterogeneous catalysts [26] and can increase the interaction between the catalyst and the support by altering the physicochemical properties. Polymer additives need to be chosen carefully so as not to hinder the catalytic process and need to be removed by heat treatment prior to the experiment. Even though many surfactant materials are commercially available, PEG is an attractive choice as an additive since its oxidation products contain no nitrogen, sulfur or phosphorous thus precluding catalyst poisoning during heat treatment [27]. There are several reports describing the use of polymer stabilizers for the preparation of the catalysts [28–30], but very few detailed studies on the surfactant-induced morphological changes and subsequent correlations with activity are reported. A fuller understanding of such relationships provides a useful means to improve catalyst performance. In this study, the CO oxidation performance (both in wet and dry conditions) of a PEG-stabilized $RuO_x/\gamma\text{-}Al_2O_3$ catalyst is compared with an un-stabilized equivalent. Detailed physical and chemical characterization of the materials has allowed us to begin to understand the connectivity between surfactant-mediated RuO_x catalyst design and activity.

2. Experimental Section

2.1. Materials

Alumina (Al_2O_3) powder (Sigma-Aldrich, St. Louis, Missouri, USA), $RuCl_3 \cdot xH_2O$ (Sigma-Aldrich), NH_3 solution (Junsei Chemical Co. Ltd., Tokyo, Japan), tetraethyl orthosilicate (TEOS,

Sigma-Aldrich), polyethylene glycol (PEG, average molecular weight 20,000 g/mol, Sigma-Aldrich) and ethyl alcohol (Daejung Chemical and Metals Co., Shiheung, Korea) were used as received.

2.2. Syntheses of Catalysts

The amount of 1 wt.% RuO_x supported on mesoporous γ-Al_2O_3 (hereafter referred to as RAWOS) was prepared using the following homogeneous precipitation procedure. Firstly, a known quantity of $RuCl_3 \cdot xH_2O$ (0.155 g) and TEOS (0.25 wt.%, also containing ethanol and water) solution were prepared and mixed (previously it has been suggested that the *in situ* formation of a minor amount of SiO_2 could improve the hardening of the oxidation catalyst without affecting its performance [31]). The solution was reacted with 25 mL, 1 M NH_3 solution (acting as a precipitating agent) at 75 °C. After 2 h, the required amount of Al_2O_3 powder (9.9 g irreducible support) was added and the mixture was stirred for a further 1 h. Following the reaction, the product was washed repeatedly with deionized water in order to remove the by-product and then heat-treated at 115 °C. The resulting powder was pressed into a pellet (approximately 8 ton weight for 1 cm diameter) and calcined at 650 °C for 24 h. In order to investigate the role of stabilizer/surfactant, a separate sample (hereafter referred to as RAWS) was prepared as above with the addition of a synthesis step in which PEG (0.5 g) was added prior to the addition of the NH_3 solution. The calcination step converted amorphous $Ru(OH)_3$ into RuO_x and removed PEG completely. Unmodified γ-Al_2O_3 was also prepared as a reference sample (hereafter referred to as ALVIR). Following the calcination, each of the pellets were crushed and sieved to obtain 2–3 mm size granules.

2.3. Catalyst Characterization

The phase purity and crystallinity of the catalysts were studied by a powder X-ray diffractometer (XRD, D/Max Ultima IIIdiffractometer, Rigaku Corporation, Tokyo, Japan) equipped with monochromatic Cu K_α radiation (wavelength, λ = 0.154 nm) operated at 40 mA and 40 kV. The surface morphology was analyzed using field emission scanning electron microscope (FESEM, JEM 1200 EX II, JEOL, Tokyo, Japan) and transmission electron microscopy with EDX attachment (TEM, TECNAI F20, Philips Corp., Eindhoven, The Netherlands). Identification of the basic chemical functional groups (and quantification of CO_2 during CO oxidation experiment) was performed by FTIR spectroscopy (IFS 66/S spectrometer, Bruker, Billerica, MA, USA). In addition, the surface of the catalysts was also characterized by using an X-ray photoelectron spectroscopy (XPS, ESCA 2000, VG Microtech, West Sussex, UK) with monochromatic Mg K_α X-ray radiation (1253.6 eV) operated at 13 kV and 15 mA as an excitation source. The Quantachrome software (version 2.11, Quantachrome Instruments, Boynton Beach, FL, USA) was used to determine the surface area and pore characteristics of the catalysts. Chemisorption measurements (temperature programmed reduction (TPR) experiments) were conducted using a gas sorption analyzer (Autosorb iQ, Quantachrome Instruments, Boynton Beach, FL, USA) to predict the catalyst dispersion. In this test, 100 mg of catalyst and a mixture of H_2 and Ar (10%) were used. The samples were pretreated and the TPR profile was recorded from room temperature to 600 °C at a steady ramping.

Exactly 10 g of the catalyst prepared as above was loaded in a tubular reactor (diameter: 1.5 cm) and then fixed inside a furnace equipped with a temperature controller. The feed gas was prepared by mixing CO, oxygen and nitrogen. The concentration of CO was fixed at 2000 ppm (parts per million, volumetric), and the oxygen concentration was varied from 0.5 to 2.5 vol.% with the total flow rate kept at 1 $L \cdot min^{-1}$. The volume of the catalyst inside the reactor was 11.48 cm^3, corresponding to a space velocity of 5226 h^{-1} at a feed gas flow rate of 1 $L \cdot min^{-1}$. All experiments were performed under isothermal conditions (the feed gases were introduced immediately after the required temperature was attained). The difference between the temperature measured at the catalyst using a thermocouple and that recorded by the temperature controller was negligible. The concentration of CO at the outlet was measured by using the FTIR spectrometer after 1 h of the reaction.

3. Results

3.1. Characterization

Figure 1 shows the FESEM micrographs of the RAWOS and RAWS catalysts. The RAWOS samples showed the presence of aggregated structures of RuO_x nanomaterials inside and on the surface of the γ-Al_2O_3 support. By contrast, the PEG-stabilized RAWS sample exhibited a finger-like protrusion of RuO_x on the surface of the γ-Al_2O_3. The TEM image of RAWOS sample (Figure 2a) clearly displayed the distinction between γ-Al_2O_3 (gray) and small size RuO_x (black) which is non-uniform in shape and size. EDX analysis was also performed in the above locations, which confirmed the particular morphological feature was due to RuO_x. At the same time, RAWS clearly showed the presence of rod-like structures with a length and width of *ca.* 200 and 75 nm, respectively (Figure 2b). Assemblies of nanorods like this were widespread throughout catalyst samples. The approximate elemental composition measured by EDX for the corresponding catalysts can be seen in the right side of the figures. The RAWOS catalyst contains 58.34% oxygen and 9.78% Ru, whereas RAWS contains 46.49% oxygen and 50.94% Ru (atomic percentage). The observed one dimensional (1D) growth found in RAWS is proposed to originate from the formation of micelles in PEG solution, which further directs the growth of the catalyst. As noted previously in the literature, the formation of 1D structure is achieved due to the effect of PEG acting as a capping and growth directing agent. The ordered chain structure of PEG (mainly arising from oxygen in the C-O-C chains) is anticipated to adsorb easily on a ruthenium-rich surface, coordinating with the ruthenium ions, forming PEG-Ru^{+3} complexes in the colloidal state and confining growth at specific crystal faces [32,33]. Subsequent neutralization with alkaline solution (ammonia) produces PEG-$Ru(OH)_3$. Finally heat treatment at high temperature (650 °C) removes PEG and water which results in the ruthenium oxide nanomaterials. This process is shown schematically in Figure 3.

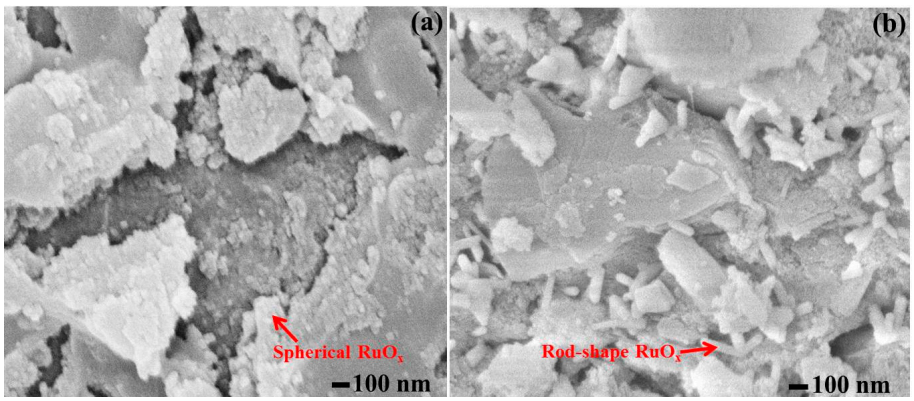

Figure 1. The FESEM surface morphological images of RAWOS (**a**) and RAWS; (**b**) catalysts. (Abbreviations: RAWOS: $RuO_x/\gamma\text{-}Al_2O_3$ without polymer stabilizer; RAWS: PEG stabilized $RuO_x/\gamma\text{-}Al_2O_3$).

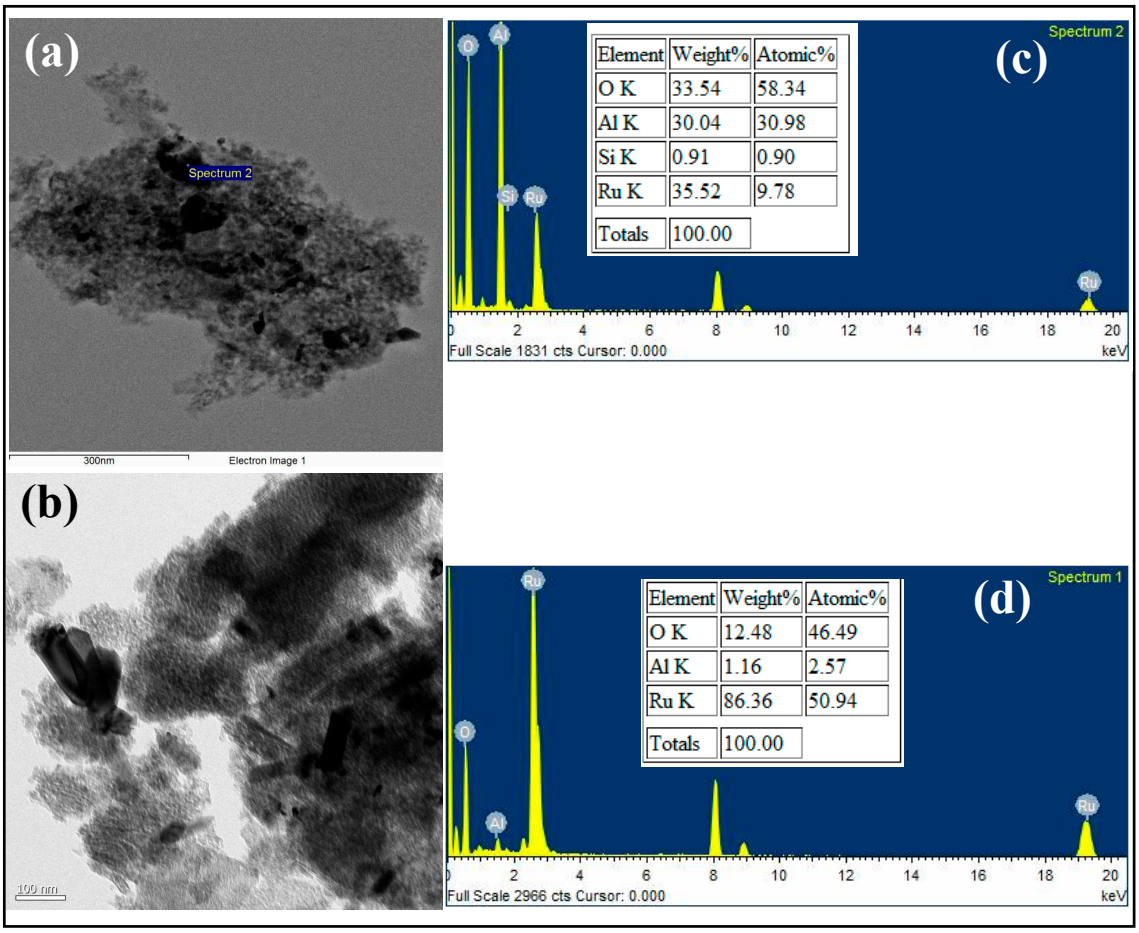

Figure 2. The TEM images of (**a**) RAWOS and (**b**) RAWS catalysts, and the EDX spectra of (**c**) RAWOS and (**d**) RAWS catalysts along with the elemental composition.

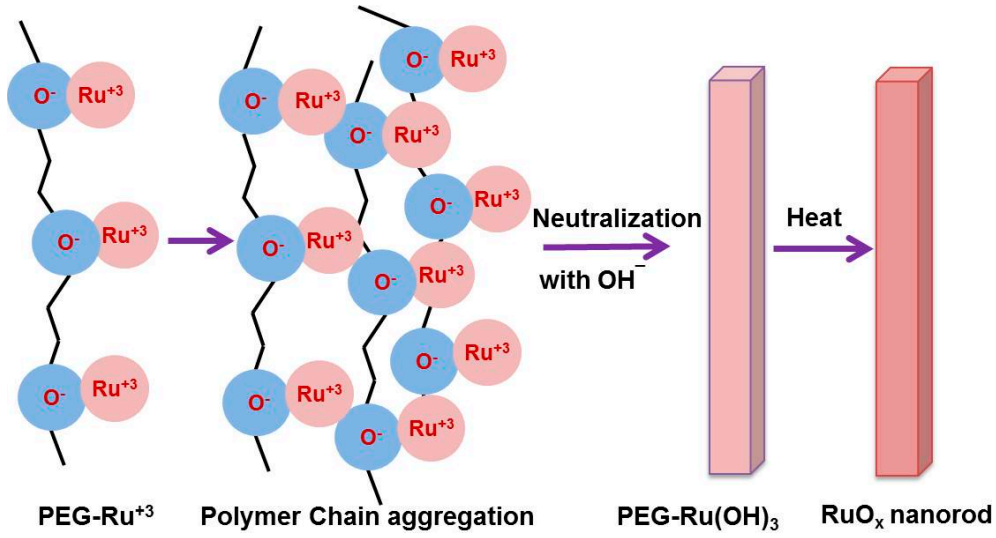

Figure 3. Formation mechanism of 1-D RuO_x in the presence of PEG.

The phase and crystal structure of the ALVIR, RAWOS and RAWS catalysts were analyzed by using XRD and given in Figure S1. The diffraction pattern of the as-received alumina shows prominent diffraction peaks at 2θ = 36.7, 45.8 and 66.9° corresponding to the (311), (400) and (440) reflections of γ-Al_2O_3, respectively (*cf.* JCPDS card no. 00-010-0425). Commonly, commercial γ-Al_2O_3 is mesoporous with a higher surface area and is the most thermodynamically stable phase of alumina [34–36]. The XRD diffractograms of both the synthesized and heat-treated catalyst materials displayed identical peaks although reflections corresponding to RuO_x could not be observed clearly, which may due to the inclusion of Ru atoms in the interstitial sites of alumina or it may simply due to the lesser amount of RuO_x (1 wt.%) [37]. In case of the X-ray diffractometer employed in this work, it was found that the catalyst loading should be greater than 7 wt.% to clearly identify RuO_x diffraction peaks and to calculate the lattice parameters.

The FTIR spectra of the ALVIR, RAWOS and RAWS catalysts are shown in Figure S2a–c, respectively. As-received alumina exhibited prominent bands at 550 cm^{-1} and 790 cm^{-1} corresponding to the Al ions in octahedral and tetrahedral surrounding (Al-O vibrations), respectively [38]. The band at 1635 cm^{-1} can be associated with physisorbed water (from exposure prior to analysis), and a broad peak between 3200 cm^{-1} and 3600 cm^{-1} indicates OH stretching exhibited by hydroxyl functional groups [39,40]. The FTIR spectra of the RAWOS and RAWS catalysts displayed similar peaks to those observed in spectra for ALVIR. Ru-O vibrations are expected to occur between 600 and 800 cm^{-1} and thus a distinction between Al-O and Ru-O bands could not be clearly made. Bands originating from the functional groups associated with PEG (the main C-O-C band at 1094 cm^{-1}) in the RAWS sample were not observed, which implies that the PEG was removed by the heat treatment.

The RAWOS and RAWS supported catalysts were additionally characterized using XPS (Figure 4). The spectra were de-convoluted by using a Gauss-Laurentzian peak fitting program. The respective high resolution core level Al 2p, Ru 3d and Ru 3p spectra are given for the catalyst RAWOS (Figure 4a–c) and RAWS (Figure 4d–f). The binding energy values observed in the Al 2p spectra of both catalysts correspond to Al_2O_3 as expected [41]. Spectra also contained peaks corresponding to carbon (284.5 eV) and Ru 3d peaks typical for ruthenium oxides (286.2 and 286.0 eV) [42]. Since the Ru 3d and C 1s peaks are very close in terms of binding energy values, spectra in the Ru 3p binding

energy region were recorded to clarify the ruthenium oxidation state and bonding environment. From the positions and relative intensity of the observed peaks, the RAWOS sample surface consisted of approximately 68 at.% Ru (IV) (typical of RuO_2; 462.4 eV) and approximately 32 at.% RuO_3 (465.0 eV) [42,43]. By comparison, Ru 3p peaks for the RAWS sample surface reflected an approximate composition of 62 at.% RuO_x (*i.e.*, higher oxides of Ru, where $x = 3$ mostly) at 464.3 eV and 38 at.% elemental Ru°, (461.8 eV) [42]. It has been reported that RuO_3 is found in all of the surfaces of RuO_2 and it plays a main role in the stability of RuO_2 [42]. It is clearly seen that when the sample was prepared with a polymer stabilizer such as PEG (as is the case for the RAWS), formation of metallic Ru is induced through the reducing activity of the stabilizer [44].

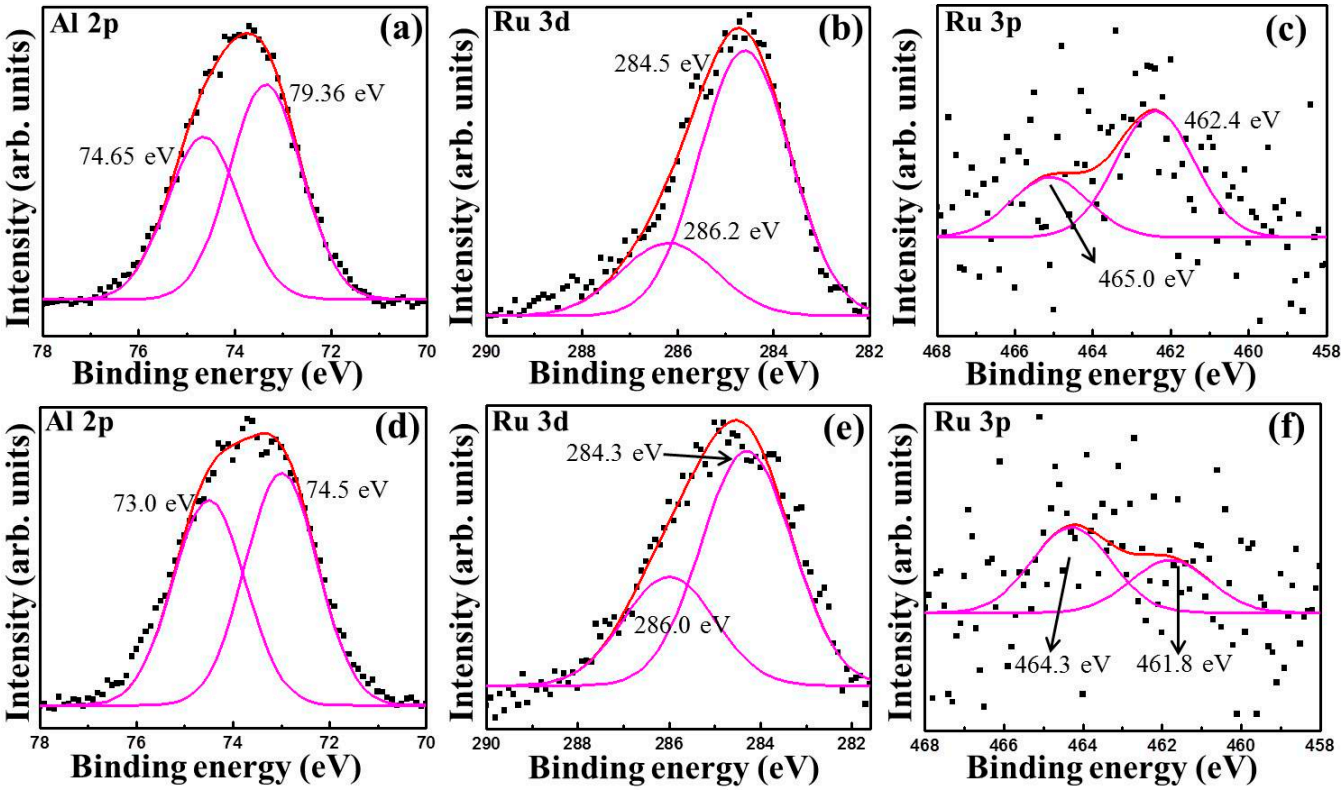

Figure 4. High resolution core level Al 2p, Ru 3d and Ru 3p spectra corresponding to RAWOS (**a**–**c**) and RAWS (**d**–**f**) catalysts.

The adsorption capacity of gas molecules within the pores of the catalyst is an important step towards understanding the catalyst reaction. This can be determined from the surface and pore-characteristics of the catalyst. Figure 5 shows the N_2 adsorption-desorption isotherm (Figure 5a–c) and the multipoint Brunauer-Emmet-Teller (BET) plots (Figure 5d–f) for the ALVIR, RAWOS and RAWS materials, respectively. From the sorption profiles it is evident that the catalysts exhibit mesoporous type IV isotherm behavior in which the intake of adsorbate increases at high pressure. The pore volume and pore radius of the catalysts during adsorption and desorption process calculated by Barrett-Joyner-Halenda (BJH) method are listed in Table 1, which confirmed the standard values of the pore size (1.5–100 nm) reported [45]. The linearity of the data (indicating a strong interaction of the ruthenium oxide catalyst with N_2) in the relative pressure (P/P_0) range of 0.0–0.3 reinforces the suitability of applying the BET model in determining the specific surface area of the catalysts.

The BET surface area is generally used for practical purposes. The ALVIR, RAWOS and RAWS catalysts exhibit BET surface area values of *ca.* 112.2, 138.3 and 128.1 $m^2 \cdot g^{-1}$, respectively. From a comparison of the RAWS and RAWOS sorption isotherm results, the addition of the polymer stabilizer apparently leads to an increase in the pore volume and pore radius and a decrease in the surface area values by 10.2 $m^2 \cdot g^{-1}$. A similar trend has been reported previously for Ni-Al_2O_3 catalyst stabilized by cetyltrimethylammonium bromide [30].

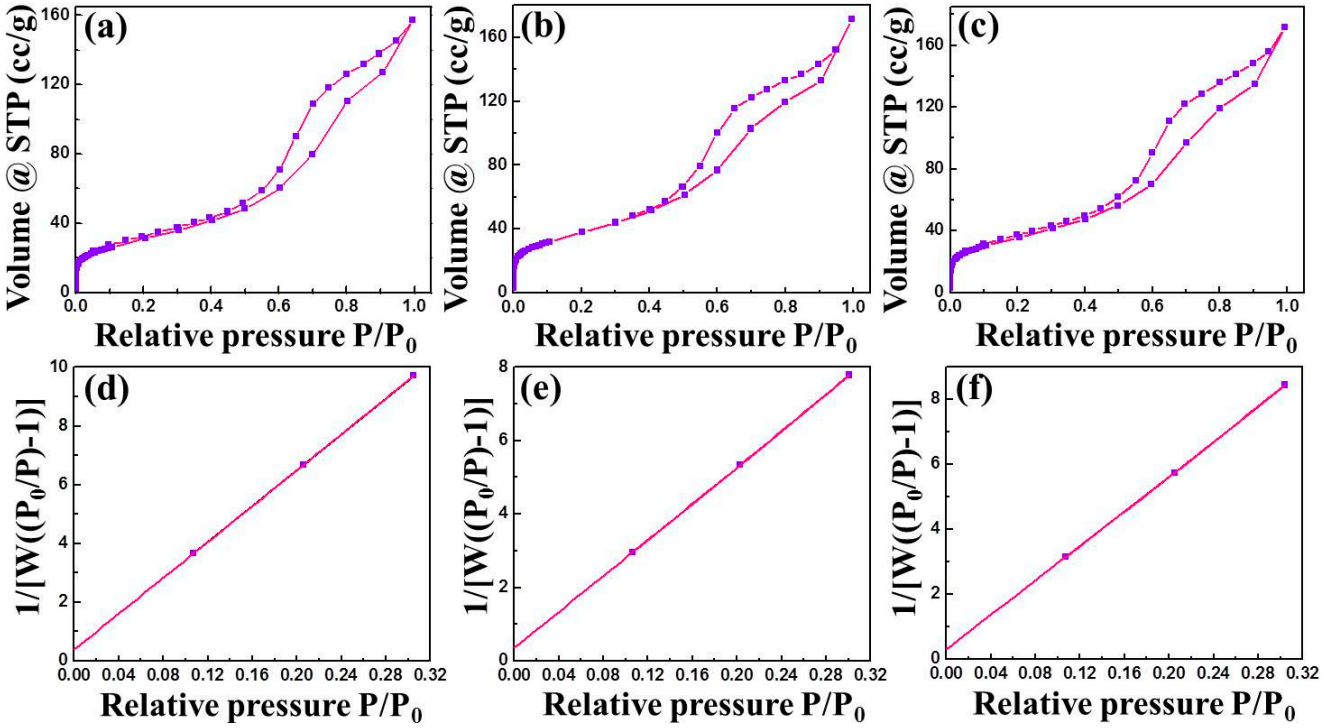

Figure 5. Nitrogen adsorption-desorption isotherms (**a**)–(**c**) and the multipoint BET plots; (**d**)–(**f**) corresponding to ALVIR, RAWOS and RAWS catalysts.

Table 1. Physisorption results of the catalysts measured by Barrett-Joyner-Halenda (BJH) method.

Catalyst Name	Process	Surface Area (m^2/g)	Pore Volume (cc/g)	Pore Radius (Mode Dv(r)) (Å)
ALVIR	Adsorption	102.9	0.2322	30.72
	Desorption	140.7	0.2480	28.18
RAWOS	Adsorption	120.5	0.2475	30.58
	Desorption	168.7	0.2694	24.40
RAWS	Adsorption	119.0	0.2532	30.76
	Desorption	164.8	0.2723	24.54

3.2. CO Oxidation Performance of the Catalysts

Oxygen concentration and temperature were varied in the range of 0.5–2.5 vol.% and 50–250 °C, respectively, in a series of CO oxidation experiments. The inlet concentration of CO was fixed at 2000 ppm. The conversion of CO into CO_2 obtained with as received γ-Al_2O_3 (ALVIR) under steady state conditions showed a maximum of 5.6% at reactor temperature of 175 °C. The CO conversion percentages using the RAWOS and RAWS catalyst materials are shown in Figure 6a–c for oxygen

concentrations of 0.5. 1.5 and 2.5 vol.%. The plots clearly demonstrate a gradual increase in CO conversion from <10% at 50 °C to 100% at 200 °C. Generally, varying the oxygen content at low temperature did not affect the overall conversion process significantly but its influence at high temperature is clear. The RAWOS catalyst exhibits substantial activity above 100 °C. Similar behavior was observed on repeating the oxidation experiments with the PEG-stabilized RAWS catalyst, but the CO conversion percentage at each experimental temperature was notably higher. Moreover, total conversion was achieved at 175 °C as compared to 200 °C observed for the equivalent RAWOS catalyst. At low temperature (50 °C and 75 °C), the difference between the materials is almost negligible but when the temperature is increased, a remarkable difference can be noted. An increase in the CO conversion efficiency of about 33% by RAWS catalyst was observed in experiments at 125 °C with an O_2 concentration of 1.5%. Above and below this temperature, a gradual decrease in the conversion efficiency can be noted with a slight variation depending on the oxygen concentration. The stability of the catalysts was also confirmed by conducting the experiments continuously for 7 h at 125 °C. These extended experiments showed the repeatability of the performance observed above without any significant change.

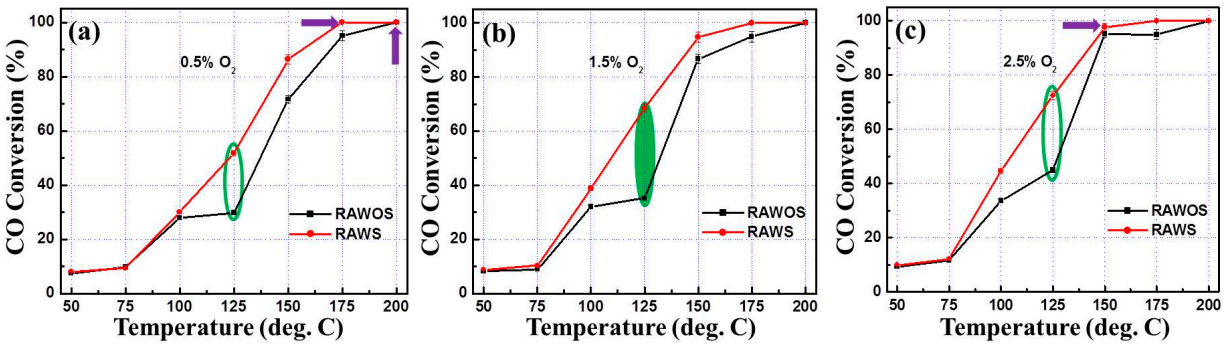

Figure 6. The CO oxidation performance of RAWOS and RAWS catalysts with different concentrations of oxygen. (**a**) 0.5 vol.%, (**b**) 1.5 vol.% and (**c**) 2.5 vol.%.

In order to investigate the performance of the catalysts under real working conditions, water vapor was added to the reactant gas (*i.e.*, CO + H_2O + O_2). The experiments were thus performed in the presence of 2.5% and 5% water (by volume) at different temperature. The results of these CO oxidation experiments are represented in Figure 7. The CO conversion efficiency increased depending upon the temperature. For a water content of 2.5%, full conversion was achieved at 275 °C for the RAWOS catalyst. By contrast, the rod type RAWS catalysts exhibited 100% CO oxidation at a reduced temperature of 225 °C (Figure 7a). Increasing the water content from 2.5% to 5% resulted in the shift of temperature to 300 °C for the RAWOS material and 250 °C for the RAWS catalyst, respectively (Figure 7b). In addition, it is very clear that at every reaction temperature, the RAWS catalyst showed an improved conversion performance over the RAWOS equivalent. As compared to the results obtained under dry conditions, the increase in the effective temperature required for full conversion can be understood in terms of the competition between CO and H_2O adsorption in the reactive sites of the catalysts. This is also consistent with the finding that pre-oxidized RuO_x catalysts are very active in dry conditions, similar to the phenomena exhibited by oxides of copper and cobalt [46,47].

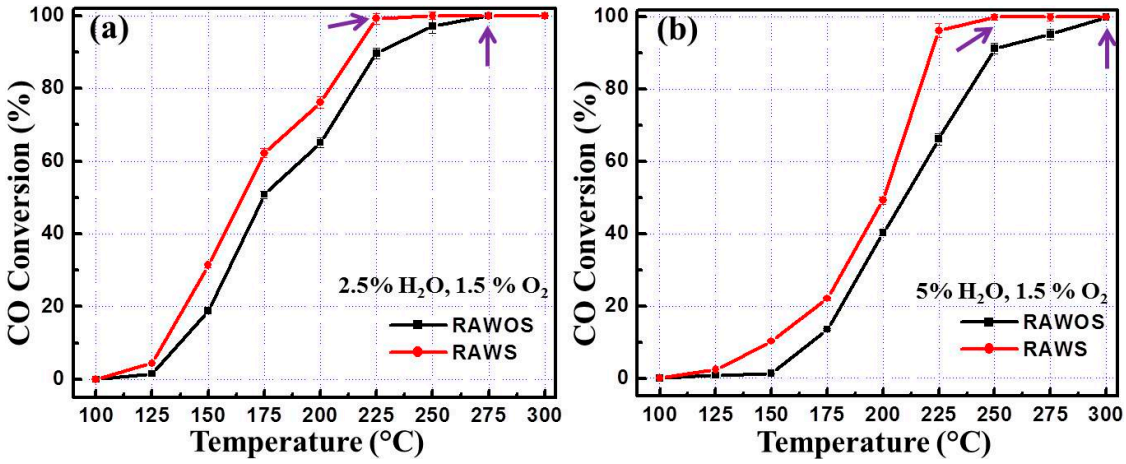

Figure 7. Effect of (**a**) 2.5 vol.% and (**b**) 5 vol.% water content on the CO oxidation performance using RAWS and RAWOS catalyst. The inlet oxygen concentration was fixed at 1.5 vol.%.

4. Discussion

The reason for the enhancement of the catalytic activity in the PEG-stabilized materials results from a combination of factors. First, the increase in the pore volume and pore size would appear to be the dominant effect (Table 1) [30]. Second, the stoichiometric and non-stoichiometric ruthenium oxides (and hence variable ruthenium oxidation states) states might be expected to contribute to the catalyst activity as is seen, for example, for MnO_x (where $x \leq 2$) [48]. Arguments in the literature suggest that metallic Ru, as observed in the RAWS material (and as found by XPS), forms bonds with adsorbed ad-layers of oxygen (as a transient surface oxide) *in situ* during CO oxidation and is catalytically more active below 500 K [49–52]. Third, metallic catalysts such as Pd and Rh on oxide supports show structure-sensitive (size) catalytic activity [46] and favor towards high CO adsorption. Zhou *et al.*, have reported that an increase in the CO oxidation capability of Pt nanowires over zero dimensional Pt nanoparticles is due to the large crystal facets and a small density of defect sites [53]. This means that the synergistic effect rendered by rod-structured RuO_x (as a manifestation of shape dependent catalytic activity) also partly explain such improvements [54]. It is reported that the difference in the geometry of nanomaterials occurs due to the changes in the surface atomic arrangement, thus exhibiting different electronic structures [55]. The binding strength between the catalyst surface and the adsorbed species (interaction) depends on such atomic arrangements (defect structures), which in turn influences the catalytic activity and selectivity [28,56,57]. The open coordination sites rendered by the edge and corner atoms [58] usually found in tetrahedral nanomaterials (in case of this work, Ru exhibits rutile-type structure with Ru atoms located in the corner) might significantly affect adsorption energy (activation energy) and bond enthalpy [59]. In addition, the flat sides of RuO_x containing large number of surface atoms would result in an increase in the contact area with the catalyst support, which can provide additional sites for the adsorption of reactant molecules [60].

Finally, the catalyst dispersion engendered in the PEG-stabilized catalysts contributes significantly to catalyst activity. Figure 8 shows the TPR profiles of the RAWOS and RAWS catalysts. The H_2 consumption profiles exhibit a number of maxima at different temperatures, implying the existence of

various Ru species on γ-Al_2O_3. The H_2-TPR for RAWOS shows reduction peaks between 100–300 °C. The narrow peaks at *ca*. 168 °C and 225 °C (and 266 °C) correspond to the reduction of RuO_3 and RuO_2 [61,62]. Low temperature peak at 110 °C refers to the formation of ruthenium from tiny RuO_2 particles (Figure 8a). By comparison, the RAWS catalyst exhibited a smooth and well defined ruthenium reduction peak with large peak area at a lower temperature (95.5 °C). The high temperature peak at 522 °C is the result of the reduction of the mesoporous γ-Al_2O_3 support [63,64] and the peak observed as a shoulder at 331 °C should be due to the reduction of large RuO_2 nanorod structures. Comparing the peak areas, the amount of H_2 gas consumed by the RAWS catalyst is higher than the un-stabilized catalyst and the reduction events are shifted consistently to lower temperature (by between 35–170 °C). One might infer therefore that since the rod-structured catalyst is well dispersed the formation of oxygen vacancies throughout the RuO_x is facilitated via the facile interaction of gaseous species, which ultimately leads to an enhancement of CO oxidation. Such a size and shape dependent reduction behavior was also reported for CeO_2 catalysts in the literature [63].

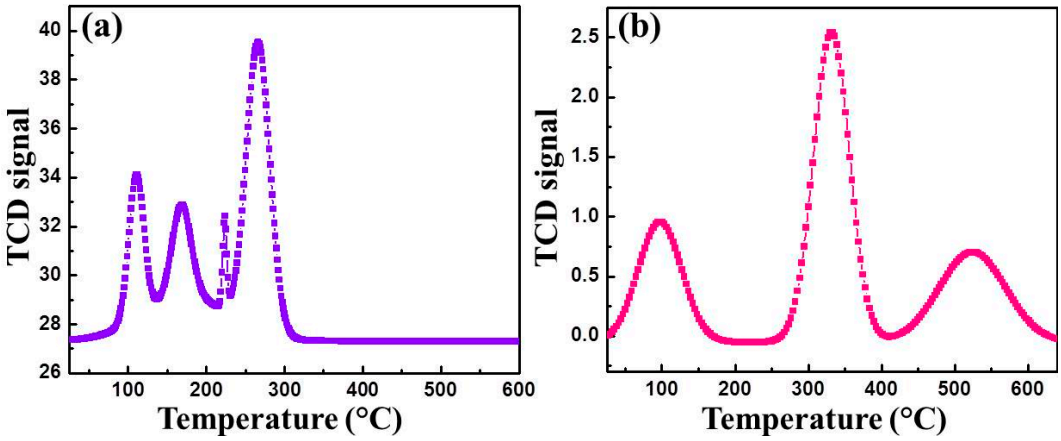

Figure 8. The H_2 consumption (TPR) profiles of the RAWOS (**a**) and RAWS (**b**) catalysts.

5. Conclusions

The preparation of nano-sized RuO_x catalysts on mesoporous γ-Al_2O_3 support was achieved following a chemical co-precipitation route. Two predominant types of catalyst nanomaterial were synthesized; aggregated spheres and dispersed rods. The addition of PEG surfactant was essential in achieving the latter catalyst morphology. Subsequent characterization showed that polymeric surfactant used for stabilization could be removed by heat treatment and did not lead to catalyst poisoning. The surfactant played the principal role in controlling the morphology and pore characteristics of the catalysts. It was observed that the PEG-stabilized rod type nanomaterials showed superior conversion over un-stabilized spherical-shaped materials in the catalytic oxidation of CO. The use of PEG in mediating the shape, size, surface structure and transition metal oxidation state is crucial in tailoring catalyst performance.

Supplementary Materials

The XRD and FTIR spectrum of the ALVIR, RAWOS and RAWS catalysts are provided.

Acknowledgments

This research was supported by Basic Science Research Program through the National Research Foundation of Korea (NRF) funded by the Ministry of Science, ICT and future Planning (Grant No. 2013R1A2A2A01067961).

Author Contributions

Antony Ananth performed the experimental work and analyzed the data; Duncan H. Gregory helped prepare the first draft of the manuscript and provided advice on the discussion; Young Sun Mok supervised all the study and participated in the interpretation of the results.

Conflicts of Interest

The authors declare no conflict of interest.

References

1. Zhan, B.Z.; White, M.A.; Sham, T.K.; Pincock, J.A.; Doucet, R.J.; Rao, K.V.R.; Robertson, K.N.; Cameron, T.S. Zeolite-confined nano-RuO2: Agreen, selective, and efficient catalyst for aerobic alcohol oxidation. *J. Am. Chem. Soc.* **2003**, *125*, 2195–2199.
2. Sugimoto, W.; Iwata, H.; Yasunaga, Y.; Murakami, Y.; Takasu, Y. Preparation of ruthenic acid nanosheets and utilization of its interlayer surface for electrochemical energy storage. *Angew. Chem. Int. Ed.* **2003**, *42*, 4092–4096.
3. Zhang, Y.; Wang, C.; Wan, N.; Mao, Z. Deposited RuO_2-IrO_2/Pt electrocatalyst for the regenerative fuel cell. *Int. J. Hydrogen Energy* **2007**, *32*, 400–404.
4. Park, S.; Kim, M.; Koo, D.H.; Chang, S. Use of ruthenium/alumina as a convenient catalyst for copper-free Sonogashira coupling reactions. *Adv. Syn. Catal.* **2004**, *346*, 1638–1640.
5. Dutta, P.K.; Vaidyalingam, A.S. Health effects of exposure to ambient carbon monoxide. *Microporous Mesoporous Mater.* **2003**, *62*, 107–120.
6. Kwon, S.-H.; Kim, K.-H. Hybrid functional RuO_2-Al_2O_3 thin films prepared by atomic layer deposition for inkjet printhead. *J. Solid State Electrochem.* **2010**, *14*, 225–229.
7. Li, K.; Wang, X.F.; Zeng, H.C. Kinetics of N_2O decomposition on a RuO_2/Al_2O_3 catalyst. *Chem. Eng. Res. Design* **1997**, *75*, 807–812.
8. Gracia-Suarez, E.J.; Tristany, M.; Gracia, A.B.; Colliere, V.; Philippot, K. Carbon-supported Ru and Pd nanoparticles: Efficient and recyclable catalysts for the aerobic oxidation of benzyl alcohol in water. *Microporous Mesoporous Mater.* **2012**, *153*, 155–162.
9. Zang, L.; Kisch, H. Room temperature oxidation of carbon monoxide catalyzed by hydrous ruthenium dioxide. *Angew. Chem. Int. Ed.* **2000**, *39*, 3921–3922.
10. Goodman, D.W.; Peden, C.H.F. CO oxidation on ruthenium: The nature of the active catalytic surface. *Surf. Sci.* **2007**, *601*, L124–L126.
11. Maeno, H.; Matsumoto, H. Alumina-supported ruthenium catalyst. US Patent 6429167, 6 August 2002.
12. Raub, J.A. Health effects of exposure to ambient carbon monoxide. *Chemosphere* **1993**, *1*, 331–351.

13. Perez, Y.; Ruiz-Gonzalez, M.L.; Gonzalez-Calbet, J.M.; Concepcion, P.; Boronat, M.; Corma, A. Shape-dependent catalytic activity of palladium nanoparticles embedded in SiO_2 and TiO_2. *Catal. Today* **2012**, *180*, 59–67.
14. Martynova, Y.; Yang, B.; Yu, X.; Boscoboinik, J.A.; Shaikhutdinov, S.; Freund, H.J. Low temperature CO oxidation on ruthenium oxide thin films at near-atmospheric pressures. *Catal. Lett.* **2012**, *142*, 657–663.
15. Mahammadunnisa, S.K.; Reddy, P.M.K.; Lingaiah, N.; Subrahmanyam, Ch. $NiO/Ce_{1-x}Ni_xO_2$-δ as an alternative to noble metal catalysts for CO oxidation. *Catal. Sci. Technol.* **2013**, *3*, 730–736.
16. Wang, R.; Wang, J.; Liu, L.; Dai, H. Mechanism for the high reactivity of CO oxidation on a ruthenium-oxide. *Catal. Today* **2013**, *201*, 68–78.
17. Liu, Z.-P.; Hu, P. Mechanism for the high reactivity of CO oxidation on a ruthenium-oxide. *J. Chem. Phys.* **2001**, *114*, 5956–5957.
18. Rosu, M.-C.; Suciu, R.-C.; Dreve, S.-V.; Silipas, T.-D.; Bratu, I.; Indrea, E. The influence of PEG/PPG and of the annealing temperature on TiO_2-based layers properties. *Rev. Roum. Chim.* **2012**, *57*, 15–21.
19. Sabori, R.; Sharifnia, S.; Aalami-Aleagha, M.E.; Panahi, M.R. Promotion of metallic catalysts by metal oxide powders in partial oxidation of methane. *J. Taiwan Inst. Chem. Eng.* **2012**, *43*, 153–158.
20. Vadakkekara, R.; Chakraborty, M.; Parikh, P.A. Room temperature benzaldehyde oxidation using air over gold-silver nanoalloy catalysts. *J. Taiwan Inst. Chem. Eng.* **2015**, *50*, 84–92.
21. Sinfelt, J.H. Structure of metal catalysts. *Rev. Modern Phys.* **1979**, *51*, 569–589.
22. Achouri, I.E.; Abatzoglou, N.; Fauteux-Lefebvre, C.; Braidy, N. Polymer-assisted fabrication of nanoparticles and nanocomposites. *Catal. Today* **2013**, *207*, 13–20.
23. Rozenberg, B.A.; Tenne, R. Polymer-assisted fabrication of nanoparticles and nanocomposites. *Prog. Polym. Sci.* **2008**, *33*, 40–112.
24. Zhang, H.; Feng, J.; Wang, J.; Zhang, M. Preparation of ZnOnanorods through wet chemical method. *Mat. Lett.* **2007**, *61*, 5202–5205.
25. Lijima, M.; Kamiya, H. Surface modification for improving the stability of nanoparticles in liquid media. *KONA Powder Part. J.* **2009**, *27*, 119–129.
26. Ananth, A.; Mok, Y.S. Synthesis of RuO_2 nanomaterials under dielectric barrier discharge plasma at atmospheric pressure — Influence of substrates on the morphology and application. *Chem. Eng. J.* **2014**, *239*, 290–298.
27. Han, S.; Kim, C.; Kwon, D. Thermal/oxidative degradation and stabilization of polyethylene glycol. *Polymer* **1997**, *38*, 317–323.
28. Kim, C.; Lee, H. Shape effect of Pt nanocrystals on electrocatalytic hydrogenation. *Catal. Comm.* **2009**, *11*, 7–10.
29. Einaga, H.; Harada, M. Photochemical preparation of poly (*N*-vinyl-2-pyrrolidone)-stabilized platinum colloids and their deposition on titanium dioxide. *Langmuir* **2005**, *21*, 2578–2584.
30. Jung, Y.-S.; Yoon, W.-L.; Rhee, Y.-W.; Seo, Y.-S. The surfactant-assisted Ni-Al2O3 catalyst prepared by a homogeneous precipitation method for CH_4 steam reforming. *Int. J. Hydrogen Energy* **2012**, *37*, 9340–9350.
31. Baldwin, R.W. Preparation of catalyst pellets having sustained hardness and attrition resistance. US Patent 3146210, 25 August 1964.

32. Ananth, A.; Dharaneedharan, S.; Gandhi, M.S.; Heo, M.-S.; Mok, Y.S. Novel RuO_2 nanosheets—Facile synthesis, characterization and application. *Chem. Eng. J.* **2013**, *223*, 729–736.
33. Vidyasagar, C.C.; ArthobaNaik, Y. Surfactant (PEG 400) effects on crystallinity of ZnO nanoparticles. *Arab. J. Chem.* **2012**, doi:10.1016/j.arabjc.2012.08.002.
34. Rozita, Y.; Brydson, R.; Scott, A.J. An investigation of commercial gamma-Al_2O_3 nanoparticles. *J. Phys.: Conf. Ser.* **2010**, *241*, 012096–012099.
35. Xu, B.; Xiao, T.; Yan, Z.; Sun, X.; Sloan, J.; Gonazalez-Cortes, S.L.; Alshahrani, F.; Green, M.L.H. Synthesis of mesoporous alumina with highly thermal stability using glucose template in aqueous system. *Microporous Mesoporous Mater.* **2006**, *91*, 293–295.
36. Sifontes, A.B.; Urbina, M.; Fajardo, F.; Melo, L.; Gracia, L.; Mediavilla, M.; Carrion, N.; Brito, J.L.; Hernandez, P.; Solano, R.; *et al*. Preparation of γ-alumina foams of high surface area employing the polyurethane sponge replica method. *Lat. Am. Appl. Res.* **2010**, *40*, 185–191.
37. Altwasser, S.; Glaser, R.; Weitkamp, J. Ruthenium-containing small-pore zeolites for shape-selective catalysis. *Microporous Mesoporous Mater.* **2007**, *104*, 281–288.
38. Macedo, M.I.F.; Osawa, C.C.; Bertran, C.A. Sol-gel synthesis of transparent alumina gel and pure gamma alumina by urea hydrolysis of aluminum nitrate. *J. Sol-Gel Sci. Technol.* **2004**, *30*, 135–140.
39. Karim, M.R.; Rahman, M.A.; Miah, M.A.J.; Ahmed, H.; Yanagisawa, M.; Ito, M. Synthesis of γ-alumina particles and surface characterization. *Open Colloid Sci. J.* **2011**, *4*, 32–36.
40. Hosseini, S.A.; Niaei, V.; Salari, D. Production of γ-Al_2O_3 from Kaolin. *Open J. Phys. Chem.* **2011**, *1*, 23–27.
41. Strohmeier, B.R. Characterization of an activated alumina Claus catalyst by XPS. *Surf. Sci. Spectra* **1994**, *3*, 141–146.
42. Shen, J.Y.; Adnot, A.; Kaliaguine, S. An ESCA study of the interaction of oxygen with the surface of ruthenium. *Appl. Surf. Sci.* **1991**, *51*, 47–60.
43. McEvoy, A.J.; Gissler, W. ESCA spectra and electronic properties of some ruthenium compounds. *Phys. Status Solidi A* **1982**, *69*, K91–K96.
44. Luo, C.; Zhang, Y.; Zeng, X.; Zeng, Y.; Wang, Y. The role of poly(ethylene glycol) in the formation of silver nanoparticles. *J. Colloid Inter. Sci.* **2005**, *288*, 444–448.
45. Niesz, K.; Yang, P.; Somorjai, G.A. Sol-gel synthesis of ordered mesoporous alumina. *Chem. Commun.* 2005, 1986–1987, doi:10.1039/B419249D.
46. Royer, S.; Durprez, D. Catalytic oxidation of carbon monoxide over transition metal oxides. *ChemCatChem* **2011**, *3*, 24–65.
47. Salek, G.; Alphonse, P.; Dufour, P.; Guillemet-Fritsch, S.; Tenailleau, C. Preparation of alumina-supported gold-ruthenium bimetallic catalysts by redox reactions and their activity in preferential CO oxidation. *Appl. Catal. B* **2014**, *147*, 1–7.
48. Carabineiro, S.A.C.; Bastos, S.S.T.; Orfao, J.J.M.; Pereira, M.F.R.; Delgado, J.J.; Figueiredo, J.L. Carbon monoxide oxidation catalysed by exotemplatedmanganese oxides. *Catal. Lett.* **2010**, *134*, 217–227.
49. Reuter, K.; Stampfl, C.; Pirovano, M.V.G.; Scheffler, M. Atomistic description of oxide formation on metal surfaces: The example of ruthenium. *Chem. Phys. Lett.* **2002**, *352*, 311–317.

50. Over, H.; Muhler, M.; Seitsonen, A.P. Comment on "CO oxidation on ruthenium: The nature of the active catalytic surface" by D.W. Goodman, C.H.F. Peden, M.S. Chen. *Surf. Sci.* **2007**, *601*, 5659–5662.
51. Goodman, D.W.; Peden, C.H.F.; Chen, M.S. Reply to comment on "CO oxidation on ruthenium: The nature of the active catalytic surface" by H. Over, M. Muhler, and A.P. Seitsonen. *Surf. Sci.* **2007**, *601*, 5663–5665.
52. Kirichenko, O.A.; Redina, E.A.; Davshan, N.A.; Mishin, I.V.; Kapustin, G.I.; Brueva, T.R.; Kustov, L.M.; Li, W.; Kim, C.H. Preparation of alumina-supported gold-ruthenium bimetallic catalysts by redox reactions and their activity in preferential CO oxidation. *Appl. Catal. B* **2013**, *134–135*, 123–129.
53. Zhou, W.-P.; Li, M.; Koenigsmann, C.; Ma, C.; Wong, S.S.; Adzic, R.R. Morphology-dependent activity of Pt nanocatalysts for ethanol oxidation in acidic media: Nanowires *versus* nanoparticles. *Electrochim. Acta* **2011**, *56*, 9824–9830.
54. Lopez, N.; Janssens, T.V.W.; Clausen, B.S.; Xu, Y.; Mavrikakis, M.; Bligaard, T.; Norskov, J.K. On the origin of the catalytic activity of gold nanoparticles for low-temperature CO oxidation. *J. Catal.* **2004**, *223*, 232–235.
55. Bratlie, K.M.; Lee, H.; Komvopoulos, K.; Yang, P.; Somorjai, G.A. Platinum nanoparticle shape effects on benzene hydrogenation selectivity. *Nano Lett.* **2007**, *7*, 3097–3101.
56. Han, J.; Kim, H.J.; Yoon, S.; Lee, H. Shape effect of ceria in Cu/ceria catalysts for preferential CO oxidation. *J. Mol. Catal. A* **2011**, *335*, 82–88.
57. Kim, Y.H.; Park, J.E.; Lee, H.C.; Choi, S.H.; Park, E.D. Active size-controlled Ru catalysts for selective CO oxidation. *Appl. Catal. B* **2012**, *127*, 129–136.
58. Zhang, D.; Niu, F.; Yan, T.; Shi, L.; Du, X.; Fang, J. Ceria nanospindles: Template-free solvothermal synthesis and shape-dependent catalytic activity. *Appl. Surf. Sci.* **2011**, *257*, 10161–10167.
59. Narayanan, R.; El-Sayed, M.A. Shape-dependent catalytic activity of platinum nanoparticles in colloidal solution. *Nano Lett.* **2004**, *4*, 1343–1348.
60. Mostafa, S.; Behafarid, F.; Croy, V.; Ono, L.K.; Li, L.; Yang, J.C.; Frenkel, A.I.; Cuenya, B.R. Shape-dependent catalytic properties of Pt nanoparticles. *J. Am. Chem. Soc.* **2010**, *132*, 15714–15719.
61. Lanza, R.; Jaras, S.G.; Canbu, P. Partial oxidation of methane over supported ruthenium catalysts. *Appl. Catal. A* **2007**, *325*, 57–67.
62. Ma, L.; He, D. Hydrogenolysis of glycerol to propanediols over highly active Ru-Re bimetallic catalysts. *Top. Catal.* **2009**, *52*, 834–844.
63. Betancourt, P.; Rives, A.; Hubaut, R.; Scott, C.E.; Goldwasser, J. A study of the ruthenium-alumina system. *Appl. Catal. A* **1998**, *170*, 307–314.
64. Bevy, L.P. *Leading Edge Catalysis Research*, 1st ed.; Nova Science Publishers, Inc: New York, NY, USA, 2005; pp. 116–117.